

# Low field phase diagram of spin-Hall effect in the mesoscopic regime

Zhenhua Qiao,<sup>1</sup> Wei Ren\*,<sup>1</sup> Jian Wang<sup>†</sup>,<sup>2</sup> and Hong Guo<sup>3</sup>

<sup>1</sup>*Department of Physics, The University of Hong Kong, Hong Kong, China*

<sup>2</sup>*Department of Physics and the center of theoretical and computational physics, The University of Hong Kong, Hong Kong, China*

<sup>3</sup>*Center for the Physics of Materials & Department of Physics, McGill University, Montreal, PQ, Canada*

When a mesoscopic two dimensional four-terminal Hall cross-bar with Rashba and/or Dresselhaus spin-orbit interaction (SOI) is subjected to a perpendicular uniform magnetic field  $B$ , both integer quantum Hall effect (IQHE) and mesoscopic spin-Hall effect (MSHE) may exist when disorder strength  $W$  in the sample is weak. We have calculated the low field “phase diagram” of MSHE in the  $(B, W)$  plane for disordered samples in the IQHE regime. For weak disorder, MSHE conductance  $G_{SH}$  and its fluctuations  $rms(G_{SH})$  vanish identically on even numbered IQHE plateaus, they have finite values on those odd numbered plateaus induced by SOI, and they have values  $G_{SH} = 1/2$  and  $rms(G_{SH}) = 0$  on those odd numbered plateaus induced by Zeeman energy. For moderate disorder, the system crosses over into a regime where both  $G_{SH}$  and  $rms(G_{SH})$  are finite. A larger disorder drives the system into a chaotic regime where  $G_{SH} = 0$  while  $rms(G_{SH})$  is finite. Finally at large disorder both  $G_{SH}$  and  $rms(G_{SH})$  vanish. We present the physics behind this “phase diagram”.

PACS numbers: 71.70.Ej, 72.15.Rn, 72.25.-b

Many recent papers have been devoted to the physics of spin-Hall effect[1] and a particular focus is the *intrinsic* spin-Hall generated in non-magnetic samples by spin-orbital interaction (SOI)[2, 3]. So far, several experimental papers have reported observations of spin-Hall effect in compound semiconductors and other systems[4]. Theoretically, it has been shown that for two dimensional (2D) samples in the clean limit, the Rashba SOI generates a spin-Hall conductivity having a universal value of  $e/8\pi$ [3]. The presence of weak disorder destroys spin-Hall effect in large samples[5, 6]. In particular, a consensus appears to have been reached in the literature that spin-Hall effect in disordered samples generated by linear Rashba SOI vanishes at the thermodynamical limit[6, 7, 8].

For *mesoscopic* samples, numerical studies have provided evidence that the *mesoscopic spin-Hall effect* (MSHE) can survive weak disorder[9, 10, 11, 12]. For a four-probe disordered sample, MSHE conductance  $G_{SH}$  and its fluctuations  $rms(G_{SH})$  have been calculated for both linear Rashba and Dresselhaus SO interactions[10, 13]. It was found[13] that when the system is in the diffusive regime, the fluctuations  $rms(G_{SH})$  take a universal value with the same order of magnitude as the average  $G_{SH}$  itself, and is independent of the system size  $L$ , the disorder strength  $W$ , the electron Fermi energy and the SO interaction strength.

The situation becomes very interesting and more complicated when a perpendicular uniform external magnetic field  $B$  is applied to the 2D sample[14]. In this case,  $G_{SH}$  and  $rms(G_{SH})$  become functions of  $B$ . Most importantly, a magnetic field  $B$  can produce edge-states which are responsible for the integer quantum Hall effect (IQHE). Similar to the well known studies of the global phase diagram of quantum Hall effect[15], it will be very useful to map out the low field “phase diagram” of MSHE

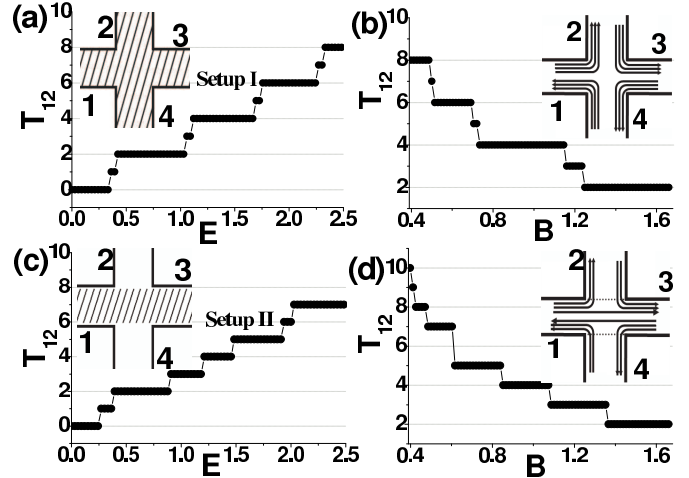


FIG. 1: Transmission coefficient  $T_{12}$  versus  $E$  or  $B(T)$ . For setup-I: (a) and (b). For setup-II: (c) and (d). Inset of (a): schematic plot of the setup-I; inset of (b): the corresponding flow of edge states. Inset of (c): schematic plot of the setup-II; inset of (d): the corresponding flow of edge states.

in terms of the field strength  $B$  and the disorder strength  $W$ . Such a diagram allows one to clearly understand the role played by the edge-states and disorder. It is the purpose of this work to present this MSHE “phase diagram” for four-probe 2D disordered mesoscopic samples with linear Rashba and/or Dresselhaus SO interactions.

Here we put “phase diagram” in quotes because the physics we study is mesoscopic, namely for samples in the coherent diffusive regime characterized by the relation between relevant length scales,  $l < L < \xi$ . Here  $L$  is the linear sample size,  $l$  the elastic mean free path and  $\xi$  the phase coherence length. As such, the “phases” in the “phase diagram” are states with zero or finite

values of  $G_{SH}$  and  $\text{rms}(G_{SH})$ , and no phase transitions are implied between these states. In particular, we found that with low disorder when IQHE is well established, both  $G_{SH}$  and  $\text{rms}(G_{SH})$  are zero identically on the *even* numbered IQHE plateaus, while they take finite values on the SOI dominant *odd* numbered IQHE plateaus. For Zeeman dominant *odd* numbered IQHE plateaus,  $G_{SH} = 1/2$  and its fluctuation vanishes. As the disorder is increased, both  $G_{SH}$  and  $\text{rms}(G_{SH})$  become nonzero when any edge-state is destroyed by the disorder in any IQHE plateau. Further increase of disorder brings the system to a “chaotic” regime where  $G_{SH} = 0$  while  $\text{rms}(G_{SH}) \neq 0$ , finally at even larger disorder both  $G_{SH}$  and  $\text{rms}(G_{SH})$  vanish. These behaviors are organized in the low field phase diagram which we determine in the rest of the paper.

We consider a 2D four-probe device schematically shown in the inset of Fig.1c (call it setup-II). A MSHE conductance  $G_{SH}$  is measured[10] across probes labeled 2, 4 when a small voltage bias is applied across probes 1 to 3 so that a current flows between them.  $G_{SH}$  can be measured the same way when there is a uniform external magnetic field  $B$  which exists everywhere including inside the leads.  $G_{SH}$  is theoretically calculated from spin-current defined as  $I_s \equiv \hbar/2(I_{\uparrow} - I_{\downarrow})$  where  $I_{\uparrow,\downarrow}$  are contributions from the two spin channels. Note that the definition of  $I_s$  is, in fact, in debate for regions where SO interaction exists[7, 16]. To avoid this ambiguity we assume that in our device the SO interaction only exists in the shaded region (setup-II in Fig.1c), namely in leads 1, 3 and in the central scattering region, but does not exist in leads 2, 4 where we measure spin-current. This way,  $I_s$  is well defined as above. For discussion purposes, we have also considered a device (setup-I, inset of Fig.1a) where SO interaction is present everywhere including inside leads 2, 4.

In the presence of linear Rashba interaction  $\alpha_{so}\mathbf{z} \cdot (\sigma \times \bar{\mathbf{k}})$  with  $\bar{\mathbf{k}} = \mathbf{k} + (e/\hbar c)\mathbf{A}$ , the Hamiltonian of the four-probe device is:

$$\begin{aligned} H = & \sum_{nm\sigma} \epsilon_{nm} c_{nm\sigma}^\dagger c_{nm\sigma} + g_s \sum_{nm\sigma\sigma'} c_{nm\sigma}^\dagger (\sigma \cdot \mathbf{B})_{\sigma\sigma'} c_{nm\sigma'} \\ & - t \sum_{nm\sigma} [c_{n+1,m\sigma}^\dagger c_{nm\sigma} e^{-im\eta} + c_{n,m-1\sigma}^\dagger c_{nm\sigma} + h.c.] \\ & - t_{so} \sum_{nm\sigma\sigma'} [c_{n,m+1\sigma}^\dagger (i\sigma_x)_{\sigma\sigma'} c_{nm\sigma'} \\ & - c_{n+1,m\sigma}^\dagger (i\sigma_y)_{\sigma\sigma'} c_{nm\sigma'} e^{-im\eta} + h.c.] \end{aligned} \quad (0.1)$$

where  $c_{nm\sigma}^\dagger$  is the creation operator for an electron with spin  $\sigma$  on site  $(n, m)$ ,  $\epsilon_{nm\sigma} = 4t$  is the on-site energy,  $t = \hbar^2/2\mu a^2$  is the hopping energy and  $t_{so} = \alpha_{so}/2a$  is the effective Rashba spin-orbit coupling,  $g_s = (1/2)g\mu_B$  (with  $g = 4$ ) is the Lande g factor. Here  $\eta = \hbar\omega_c/2t$  and  $\omega_c \equiv eB/\mu c$  is the cyclotron frequency. Throughout this paper, we use  $t$  as the unit of energy. For  $L = 40a = 1\mu m$ ,  $t = 1.5 \times 10^{-3} eV$ , and  $t_{so} = 0.2t$  corresponds to  $\alpha_{so} =$

$9 \times 10^{-12} eV.m$ [14]. We choose  $\mathbf{A} = (-By, 0, 0)$  so that the system has translational symmetry along x-direction (from lead 1 to lead 3). Static Anderson-type disorder is added to  $\epsilon_i$  with a uniform distribution in the interval  $[-W/2, W/2]$  where  $W$  characterizes the strength of the disorder. The spin Hall conductance  $G_{sH}$  is calculated from the Landauer-Buttiker formula[9]

$$G_{sH} = (e/8\pi)[(T_{2\uparrow,1} - T_{2\downarrow,1}) - (T_{2\uparrow,3} - T_{2\downarrow,3})] \quad (0.2)$$

where transmission coefficient is given by  $T_{2\sigma,1} = \text{Tr}(\Gamma_{2\sigma} G^r \Gamma_1 G^a)$ . Here  $G^{r,a}$  are the retarded and advanced Green's functions of central disordered region of the device which we evaluate numerically. The quantities  $\Gamma_{i\sigma}$  are the line width functions describing coupling of the leads to the scattering region and are obtained by calculating self-energies due to the semi-infinite leads using a transfer matrices method[17]. The spin-Hall conductance fluctuation is defined as  $\text{rms}(G_{sH}) \equiv \sqrt{\langle G_{sH}^2 \rangle - \langle G_{sH} \rangle^2}$ , where  $\langle \dots \rangle$  denotes averaging over an ensemble of samples with different disorder configurations of the same strength  $W$ . The devices in Fig.1 have  $L \times L$  central square, and without losing generality we fixed  $L = 40$  grid points in our numerics.

Before presenting the numerically determined “phase diagram” for the physics of MSHE using setup-II, let's first discuss the general physics of spin-Hall current. For this purpose we use setup-I where the SOI is everywhere so that the discussion is simpler. We first examine the spin-Hall “phase diagram” in the absence of SOI. In a magnetic field, edge-states are formed. Fig.1a,b shows transmission coefficient  $T_{12}$  for setup-I, which measures the number of edge-states, versus Fermi energy  $E$  or magnetic field  $B$ . We observe that  $T_{12}$ , or the number of edge-states, increases as  $E$  for a fixed  $B$  and it decreases as  $B$  is increased for a fixed  $E$ . Notice that the number of edge-states  $N$  can be either even or odd. The odd  $N$  region in  $E$  or  $B$  is very narrow and is due to the Zeeman splitting that breaks the spin degeneracy. When  $N$  is even, spin-Hall current vanishes because all the edge-states are fully polarized with half of them pointing to one direction (say spin-up) and the other half pointing to opposite direction (spin-down). When  $N$  is odd, the spin-Hall conductance is  $1/2$ . At weak disorder when all the edge-states survive, we therefore conclude that  $G_{sH} = 0$  when  $N$  is even and  $G_{sH} = 1/2$  when  $N$  is odd. Furthermore, it is useful to examine fluctuations of the spin-Hall conductance  $\text{rms}(G_{sH})$  for these edge-states: we expect no fluctuations for all edge-states. As disorder strength  $W$  is increased, we reach a point where at least one of the edge-states is destroyed and the system is in a spin-Hall liquid state characterized by  $G_{sH} \neq 0$  and  $\text{rms}(G_{sH}) \neq 0$  for any  $N$ . Further increasing  $W$ , we expect strong scattering to bring the system into a chaotic state of MSHE, characterized by  $G_{sH} = 0$  and  $\text{rms}(G_{sH}) \neq 0$ . At even larger  $W$ , the system enters a

spin-Hall insulator state where  $G_{sH} = \text{rms}(G_{sH}) = 0$ .

Next, we turn on the SOI and discuss its effect on the “phase diagram”. Fig.1c,d show transmission coefficient  $T_{12}$  for setup-I versus  $E$  or  $B$  for a fixed Rashba SOI  $t_{so} = 0.2$ . We observe that the behavior of  $T_{12}$  is similar to that of Fig.1a,b except that the region of odd  $N$  is now much larger. When  $N$  is even, spin-Hall current vanishes as before. In the region of  $B$  when  $N$  is odd, two cases occur due to the competition between SOI which tends to randomize the spin polarization and the Zeeman energy which favors spin polarization along a fixed direction. If Zeeman energy is large enough, then  $G_{sH} = 1/2$  as before with  $\text{rms}(G_{sH}) = 0$  while if SOI dominates then there is at least one edge-state that has both spin-up and down components: our numerical results show that the composition depends on systems parameters. As a result, there is a net spin-Hall current when  $N$  is odd. This discussion becomes clearer when we examine setup-II where the spin direction can be defined. At weak disorder when all the edge-states survive, we have the same conclusion as before, *i.e.*  $G_{sH} = 0$  when  $N$  is even and  $G_{sH} \neq 0$  when  $N$  is odd. We expect no fluctuations for even  $N$  and for those odd  $N$  edge-states with  $G_{sH} = 1/2$ , but finite fluctuations for the rest of odd  $N$  edge-states. Hence, at weak disorder, we have a “phase” of edge-state induced spin-Hall insulator with even  $N$  characterized by  $G_{sH} = \text{rms}(G_{sH}) = 0$ ; a “phase” of edge-state induced spin-Hall liquid (but fluctuationless and Zeeman dominant) with odd  $N$  characterized by  $G_{sH} = 1/2$  and  $\text{rms}(G_{sH}) = 0$ ; and finally a “phase” of edge-state induced spin-Hall liquid (SOI dominant) with odd  $N$  characterized by  $G_{sH} \neq 0$  and  $\text{rms}(G_{sH}) \neq 0$ . As we increase the disorder strength, the “phase diagram” evolves through three regimes similar to the case when SOI is off: a spin-Hall liquid regime, a chaotic regime, and a spin-Hall insulating regime.

The discussion in the last paragraph gives the entire expectation for the low field MSHE “phase diagram”. The problem of this discussion is that the spin-Hall current is not well defined in regions where SO interaction exists[7, 16] such as setup-I of Fig.1a. Therefore, in the rest of the work we consider setup-II where SO interaction does not exist in leads 2, 4 so that spin-Hall current is well defined and measurable without ambiguity. The extra complication of setup-II is that there is an interface between spatial region with  $t_{so} = 0$  and that with  $t_{so} \neq 0$ . This interface acts as a potential barrier causing additional scattering of edge-states. In particular, at certain energies one of the edge-states goes directly from lead 1 to lead 3 due to this interface scattering. Insets of Fig.1b and Fig.1d show schematically the edge states for setup-I and II, respectively. In the inset of Fig.1d, however, an edge-state is now transmitted directly from lead 1 to lead 3 due to the interface scattering just discussed. We have confirmed that this is a generic feature which occurs at different Fermi energies. For a fixed Fermi en-

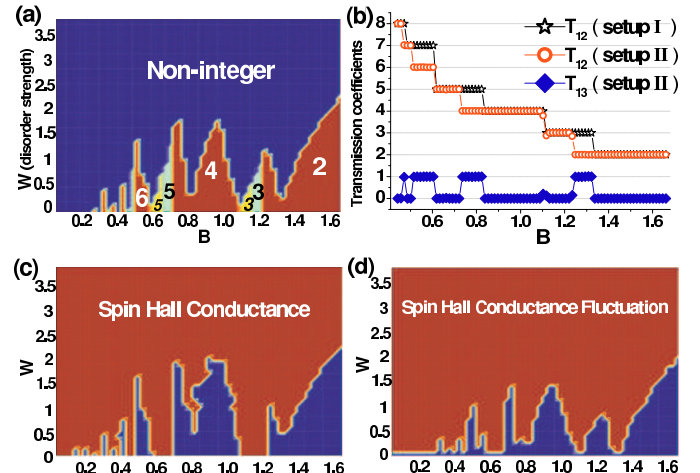


FIG. 2: (color online) (a). The edge state plateaus in  $(B, W)$  plane. (b). The transmission coefficient  $T_{12}$  for setup-I, setup-II, as well as direct transmission coefficient  $T_{13}$  as a function of  $B$  in the absence of disorder. (c). The spin-Hall conductance in  $(B, W)$  plane. (d). The spin-Hall conductance fluctuation in  $(B, W)$  plane.

ergy, this can also happen when  $B$  is varied. In Fig.2b, we plot the  $T_{12}$  for setup-I, and  $T_{12}$ ,  $T_{13}$  for setup-II, at  $W = 0$ . We observe that  $N = \text{odd}$  edge-states are much easier to be scattered while the  $N = \text{even}$  edge-states are stable against interface scattering. Therefore, the regions in the MSHE “phase diagram” where  $N = \text{even}$  becomes larger for setup-II than for setup-I. For instance, the magnetic field  $B$  for the onset of  $N = 2$  edge-state changes from 1.32T to 1.2T due to the interface scattering (for a device with lead width  $L = 1\mu\text{m}$ ). We emphasize that except for this extra complication of interface scattering in setup-II, the general physics discussion of MSHE “phase diagram” for setup-I in the last paragraph, holds perfectly for setup-II.

Fig.2a depicts numerical result for the number of edge-states  $N$  as we vary  $B$  and  $W$ . We observe that the edge-states are gradually destroyed from the subband edge (measured in the lead 1) to the subband center when  $W$  is increased. From Fig.2a we also observe that  $N = 2$  edge-states are more stable against disorder than that of  $N = 3$ . Fig.2c,d show spin-Hall conductance and spin-Hall conductance fluctuation, respectively, for  $W \leq 4$ [18]. They are perfectly consistent with the general discussion given above, namely  $G_{sH}$  and  $\text{rms}(G_{sH})$  are finite for  $N = \text{odd}$  edge-states and in regions when at least one edge-state is destroyed by disorder.

Fig.3 plots the main result of this work, the low field “phase diagram” of MSHE. In the numerical calculations of this “phase diagram”, we have computed 61 values of  $B$ , 40 values of  $W$  from  $W = 0$  to  $W = 4$ , and for each pair of  $(B, W)$  we averaged over 1000 impurity configurations. The integers in the “phase diagram” indicate the number of edge-states  $N$ . At weak disorder, there

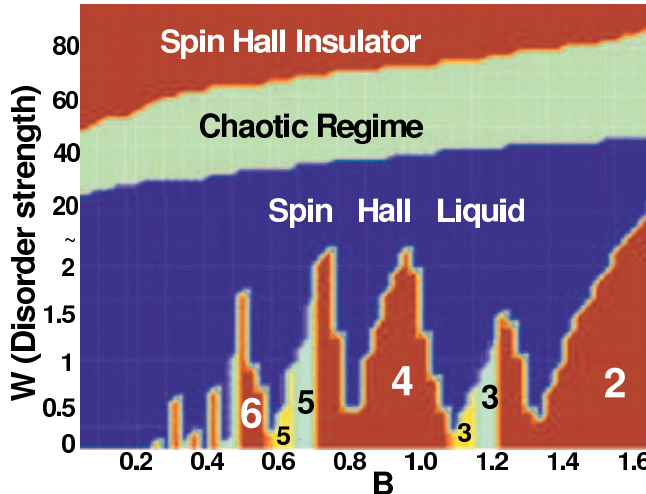


FIG. 3: (color online) The low field “phase diagram” of mesoscopic spin-Hall effect in  $(B, W)$  plane. Note that for disorder strength between  $W = 2$  to  $W = 20$ , the system is the spin-Hall liquid.

are three possible states: the  $N =$  even edge-state induced spin-Hall insulator, the SOI dominant  $N =$  odd edge-state induced spin-Hall liquid state, and the Zeeman dominant  $N =$  odd edge-state induced fluctuationless spin-Hall liquid. Since large magnetic field favors Zeeman term, so in  $N =$  odd plateau the SOI dominant spin-Hall liquid appears first for low magnetic field and crosses over to Zeeman dominant fluctuationless spin-Hall liquid at higher field. As  $W$  increases, the edge-states become destroyed and the system enters spin-Hall liquid where  $G_{sH} \neq 0$  and  $rms(G_{sH}) \neq 0$ . A chaotic state of MSHE with  $G_{sH} = 0$  and  $rms(G_{sH}) \neq 0$  is reached when  $W$  is increased further. Finally, the system enters a spin-Hall insulator state where  $G_{sH} = 0 = rms(G_{sH})$  at large enough disorder. While this “phase diagram” is obtained for a particular value of Rashba SO interaction  $t_{so}$ , we have checked that the general topology is the same for other values. In addition, the MSHE “phase diagram” in the  $(t_{so}, W)$  plane for a fixed magnetic field has similar features. We have also determined the phase boundary between the chaotic state of MSHE and spin-Hall insulator that are shown in Fig.3 with the same resolution[18].

We have so far focused on linear Rashba SOI. A similar analysis can be carried out for Dresselhaus SOI by adding a term  $\beta_{so}(\sigma_x \bar{k}_x - \sigma_y \bar{k}_y)$  in Eq.(0.1). It is well known that in the absence of Zeeman energy one has  $I_{sH}^z(\alpha_{so} = 0, \beta_{so}) = I_{sH}^z(\alpha_{so}, \beta_{so} = 0)$  and  $I_{sH}^z(\alpha_{so} = \beta_{so}) = 0$ . Therefore, in the absence of Zeeman energy, the MSHE “phase diagram” for Dresselhaus SOI is the same as that of the Rashba SOI. In the presence of Zeeman energy, our numerical results for Dresselhaus SOI give a similar “phase diagram”. When both Rashba and Dresselhaus terms are present, a similar “phase diagram”

is also obtained numerically for  $t_{so} = 0.2$  and  $t_{so2} = 0.4$  ( $t_{so2} = \beta_{so}/2a$ ).

In summary, we have determined the low field “phase diagram” of mesoscopic spin-Hall effect. The “phase diagram” is characterized by values of  $G_{sH}$  and  $rms(G_{sH})$  in the  $(B, W)$  plane and the main features include a spin-Hall liquid behavior where both  $G_{sH}$  and  $rms(G_{sH})$  are nonzero, and by spin-Hall insulator behavior where both quantities vanish. Furthermore, the spin-Hall liquid can be induced by  $N =$ odd edge-states in weak disorder, and by destroying edge-states for larger disorder. The spin-Hall insulator behavior, on the other hand, is induced by  $N =$ even edge-states, and by very large disorder. The MSHE “phase diagram” is found to be true for both linear Rashba and Dresselhaus SO interactions.

This work was financially supported by RGC grant (HKU 7048/06P) from the government SAR of Hong Kong. H.G is supported by NSERC of Canada, FQRNT of Québec and Canadian Institute of Advanced Research. Computer Center of The University of Hong Kong is gratefully acknowledged for the High-Performance Computing assistance.

\* Present address: Physics Department, Hong Kong University of Science and Technology, Clear Water Bay, Hong Kong

† Electronic address: jianwang@hkusub.hku.hk

---

- [1] J.E. Hirsch, Phys. Rev. Lett. **83**, 1834 (1999).
- [2] S. Murakami et al, Science **301**, 1348 (2003).
- [3] J. Sinova et al, Phys. Rev. Lett. **92**, 126603 (2004).
- [4] Y.K. Kato et al, Science **306**, 1910 (2004); J.Wunderlich et al, Phys. Rev. Lett. **94**, 047204 (2005); S.O. Valenzuela and M. Tinkham, Nature **442**, 176 (2006); X.D. Cui, et al, cond-mat/0608546.
- [5] J. Inoue et al, Phys. Rev. B **70**, 041303 (2004).
- [6] E.G. Mishchenko et al, Phys. Rev. Lett. **93**, 226602 (2004).
- [7] N. Sugimoto et al, Phys. Rev. B **73**, 113305(2006).
- [8] K. Nomura et al, Phys. Rev. B **73**, 113305(2006).
- [9] E.M. Hankiewicz et al, Phys. Rev. B **70**, 241301 (2004).
- [10] L. Sheng et al, Phys. Rev. Lett. **94**, 016602 (2005).
- [11] B.K. Nikolic et al, Phys. Rev. B **72**, 075361 (2005).
- [12] D. N. Sheng et al, Phys. Rev. B **72**, 153307 (2005).
- [13] W. Ren et al., Phys. Rev. Lett. **97**, 066603 (2006).
- [14] S.Q. Shen et al, Phys. Rev. Lett. **92**, 256603 (2004); Phys. Rev. B **71**, 155316 (2005).
- [15] S. Kivelson et al, Phys. Rev. B **46**, 2223 (1992). See also, D.Z. Liu et al, Phys. Rev. Lett. **76**, 975 (1996).
- [16] J.R. Shi et al, Phys. Rev. Lett. **96**, 076604 (2006).
- [17] M.P. López-Sancho, J.M. López-Sancho, and J. Rubio, J. Phys. F **14**, 1205 (1984); **15**, 851 (1985).
- [18] In our numerics, the spin-Hall conductance is taken as zero if  $G_{sH} < 0.002e/4\pi$ . The same criterion is applied to the spin-Hall conductance fluctuation.